

COMPUTATION OF PER-UNIT-LENGTH INTERNAL IMPEDANCE OF A MULTILAYER CYLINDRICAL CONDUCTOR WITH POSSIBLE DIELECTRIC LAYERS

Dino Lovrić, Slavko Vujević, Ivan Krolo

University of Split, Faculty of Electrical Engineering, Mechanical Engineering
and Naval Architecture, Split, Croatia

Abstract. *In this manuscript, a novel method for computation of per-unit-length internal impedance of a cylindrical multilayer conductor with conductive and dielectric layers is presented in detail. In addition to this, formulas for computation of electric and magnetic field distribution throughout the entire multilayer conductor (including dielectric layers) have been derived. The presented formulas for electric and magnetic field in conductive layers have been directly derived from Maxwell equations using modified Bessel functions. However, electric and magnetic field in dielectric layers has been computed indirectly from the electric and magnetic fields in contiguous conductive layers which reduces the total number of unknowns in the system of equations. Displacement currents have been disregarded in both conductive and dielectric layers. This is justifiable if the conductive layers are good conductors. The validity of introducing these approximations is tested in the paper versus a model that takes into account displacement currents in all types of layers.*

Key words: *internal impedance, multilayer cylindrical conductor, dielectric layers, conductive layers, modified Bessel functions.*

1. INTRODUCTION

Conductors composed of different types of materials are often used in a number of engineering applications [1,2]. Since each material used in the conductor has certain advantages and disadvantages, by carefully combining different types of conductor materials one can obtain a structure in which advantages of one material used negates the disadvantages of another material. However, the resulting multilayer structure becomes more challenging to accurately model. This is for example the case when performing various electromagnetic compatibility analyses [3,4], harmonic and transient analyses of transmission lines [5] as well as harmonic and transient analyses of grounding systems [6,7].

Received March 27, 2020; received in revised form May 25, 2020

Corresponding author: Dino Lovrić

Faculty of Electrical Engineering, Mechanical Engineering and Naval Architecture, R. Boskovicica 32, 21 000 Split, Croatia

E-mail: dlovric@fesb.hr

In order to obtain the distribution of electric and magnetic fields inside the multilayer structure, authors in the available literature mainly utilize a cascade of two-port networks [8-10]. This approach leads to certain numerical instabilities that are inherent to the transfer matrix of the system, where some elements of the matrix tend to infinity for high frequencies even for extra thin layers, which was demonstrated in [11]. In paper [11], however, the authors derive the equations for computation of electric and magnetic field distribution within the multilayer structure directly from Maxwell equations and base the solutions on modified Bessel functions [12] which have proven to be the most numerically stable choice [13-15]. Accurate distribution in all layers is obtained by forming a system of linear equations from boundary conditions which is then easily solved. The formulas are derived to maximize numerical stability and robustness of the proposed algorithm. In the model from [11] all layers of the multilayer conductor are characterized by electrical conductivity, permittivity and permeability, hence both conductive and displacement currents have been taken into account in all types of layers.

In this paper, a slightly different approach to model a multilayer structure is proposed and tested. First of all, the multilayer structure consists of two types of layers: conductive layers which consist of materials that are good conductors and dielectric layers, unlike in [11] where the layers are general. The proposed model consists of an arbitrary number of conductive layers where a single dielectric layer can be situated between two conductive layers. Secondly, displacement currents have been disregarded in all layers. This is only possible if the conductive layers are made of materials which are good electrical conductors. And thirdly, in the proposed model, the conductive layers are the only layers which contribute to the formation of the system of equations. Distribution of electric and magnetic fields in dielectric layers is computed indirectly from the border conditions on contiguous conductive layers. The effect of introducing these simplifications is tested in the numerical examples part of the manuscript.

2. MODEL OF THE MULTILAYER CYLINDRICAL CONDUCTOR WITH DIELECTRIC LAYERS

The multilayer cylindrical conductor analyzed in this paper can have an arbitrary number of conductive layers (m). In addition to this, the model of the multilayer conductor allows the existence of a single dielectric layer between two conductive layers, which means that for a total number of m conductive layers there can be a maximum of $m-1$ dielectric layers (the last layer of the conductor is a conductive layer).

An arbitrary i -th conductive layer is characterized by its internal radius r_i^{in} , external radius r_i^{ex} , electrical conductivity σ_i and magnetic permeability μ_i , whereas each of the dielectric layers is defined by its magnetic permeability μ_i^d and, indirectly, by the external and internal radii of the contiguous conductive layers. Electrical permittivity is non-existent in the model since the displacement currents have been disregarded in all layers. All layer materials are considered to be linear, isotropic and the parameters describing them are not frequency dependent. To better illustrate this, Fig. 1 depicts the i -th and $(i+1)$ -th conductive layers. The i -th dielectric layer illustrated on Fig. 1 is defined by the external radius of the i -th conductive layer and the internal radius of the $(i+1)$ -th conductive layer. In the case that the dielectric layer is nonexistent then $r_i^{ex} = r_{i+1}^{in}$. The developed formulas have been derived in such a way to directly take this case into account without modification. Due to simplicity

of the model, to each i -th conductive layer, where $i = 1, 2, \dots, m-1$, an i -th dielectric layer has been joined, which can be an actual dielectric layer or a fictive dielectric layer. The last conductive layer does not have a joined dielectric layer.

If the first layer is solid, then $r_j^{in} = 0$, whereas if it is a tubular, then $r_j^{in} \neq 0$.

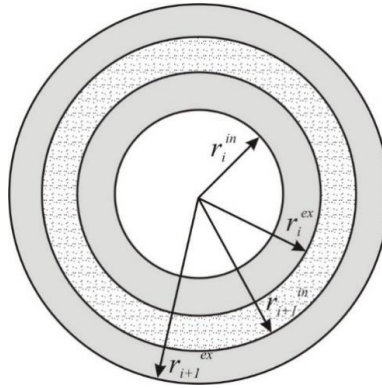


Fig. 1 Dielectric layer between two conductive layers

3. DISTRIBUTION OF ELECTRIC AND MAGNETIC FIELD IN CONDUCTIVE AND DIELECTRIC LAYERS

The formulas for the computation of electric and magnetic field inside an arbitrary i -th conductive layer of the multilayer conductor are derived directly from Maxwell equations for good conductors. Due to axial symmetry, the electric field only has the component in the direction of the conductor current whereas the magnetic field only has the azimuthal component. Unlike in paper [11], in this paper, displacement currents have been disregarded in the entire multilayer conductor including dielectric layers due to the fact that they are significantly smaller in relation to conductive currents even for higher frequencies, if the conductive layers can be considered good conductors. The effect of disregarding displacement currents will be tested in the numerical examples section of this paper.

The expressions for computation of electric and magnetic field inside an arbitrary i -th **conductive** layer are derived directly from Maxwell equations using modified Bessel functions [12] with disregarded displacement currents. For improved numerical stability of the electromagnetic models modified Bessel functions have been scaled up/down to produce values of similar order of magnitude thus avoiding any underflow/overflow numerical problems [13-15]:

$$\bar{I}_0^s(\bar{\gamma}_i \cdot r) = \exp(-\bar{\gamma}_i \cdot r) \cdot \bar{I}_0(\bar{\gamma}_i \cdot r) ; \bar{I}_1^s(\bar{\gamma}_i \cdot r) = \exp(-\bar{\gamma}_i \cdot r) \cdot \bar{I}_1(\bar{\gamma}_i \cdot r) \quad (1)$$

$$\bar{K}_0^s(\bar{\gamma}_i \cdot r) = \exp(\bar{\gamma}_i \cdot r) \cdot \bar{K}_0(\bar{\gamma}_i \cdot r); \bar{K}_1^s(\bar{\gamma}_i \cdot r) = \exp(\bar{\gamma}_i \cdot r) \cdot \bar{K}_1(\bar{\gamma}_i \cdot r) \quad (2)$$

Expressions for computation of electric and magnetic field inside an arbitrary i -th conductive layer written using scaled modified Bessel functions are:

$$\bar{H}_i = \bar{I}_{tot} \cdot \left\{ \bar{C}_i^s \cdot \bar{I}_1^s(\bar{\gamma}_i \cdot r) \cdot \exp[-\bar{\gamma}_i \cdot (r_i^{ex} - r)] + \bar{D}_i^s \cdot \bar{K}_1^s(\bar{\gamma}_i \cdot r) \cdot \exp[-\bar{\gamma}_i \cdot (r - r_i^{in})] \right\} \quad (3)$$

$$\bar{E}_i = \frac{\bar{I}_{tot} \cdot \bar{\gamma}_i}{\sigma_i} \cdot \left\{ \bar{C}_i^s \cdot \bar{I}_0^s(\bar{\gamma}_i \cdot r) \cdot \exp[-\bar{\gamma}_i \cdot (r_i^{ex} - r)] - \bar{D}_i^s \cdot \bar{K}_0^s(\bar{\gamma}_i \cdot r) \cdot \exp[-\bar{\gamma}_i \cdot (r - r_i^{in})] \right\} \quad (4)$$

$$\bar{\gamma}_i = \sqrt{\omega \cdot \mu_i \cdot \sigma_i} \cdot \exp\left(j \cdot \frac{\pi}{4}\right) = \alpha_i \cdot (1 + j) \quad (5)$$

where \bar{I}_0^s is the scaled complex-valued modified Bessel function of the first kind of order zero, \bar{K}_0^s is the scaled complex-valued modified Bessel function of the second kind of order zero, \bar{I}_1^s is the scaled complex-valued modified Bessel function of the first kind of order one, \bar{K}_1^s is the scaled complex-valued modified Bessel function of the second kind of order one, \bar{C}_i^s and \bar{D}_i^s are the unknown scaled complex-valued coefficients for the i -th conductive layer, $\bar{\gamma}_i$ is the complex wave propagation constant of the i -th conductive layer, σ_i is the electrical conductivity of the i -th conductive layer, μ_i is the magnetic permeability of the i -th conductive layer, ω is the circular frequency of the conductor current, α_i is the attenuation constant of the i -th conductive layer, \bar{I}_{tot} represents the phasor of the total multilayer conductor current and r is the distance of the observation point from the axis of the multilayer cylindrical conductor.

Computation of electric and magnetic field inside a **dielectric** layer between the i -th and $(i+1)$ -th conductive layers is achieved indirectly, from the values of electric and magnetic fields on the outer edge of the i -th conductive layer.

Computation of magnetic field at an observation point located inside a dielectric layer between the i -th and $(i+1)$ -th conductive layers is performed using Ampere's law disregarding the displacement currents. The magnetic field intensity in the dielectric layer is integrated along a curve (circle of radius r with the center located on the axis of the conductor) which produces the following equation:

$$\bar{H}_i^d \cdot 2 \cdot \pi \cdot r = \bar{I}_{enc} \quad (6)$$

where \bar{H}_i^d is the magnetic field inside the dielectric layer and \bar{I}_{enc} is the harmonic current enclosed inside the circle of radius r .

Since the magnetic field on the outer edge of the i -th conductive layer encloses the same amount of harmonic current and can be written as:

$$\bar{H}_i \Big|_{r=r_i^{ex}} \cdot 2 \cdot \pi \cdot r_i^{ex} = \bar{I}_{enc} \quad (7)$$

by introducing (7) into (6), the following equation is obtained for computation of magnetic field inside a dielectric layer between the i -th and $(i+1)$ -th conductive layers:

$$\bar{H}_i^d = \bar{H}_i \Big|_{r=r_i^{ex}} \cdot \frac{r_i^{ex}}{r} \quad (8)$$

As for the computation of electric field inside the dielectric layer between the i -th and $(i+1)$ -th conductive layers, Fig. 2 clearly describes how this is achieved. The dash-dotted line represents the axis of the multilayer conductor which lies on the z -axis of the

coordinate system. The black rectangle in the figure represents the curve over which the line integral of the electric field intensity present in the Faraday's law of induction is integrated, the black arrow denoting the positive path of integration as dictated by the right hand rule.

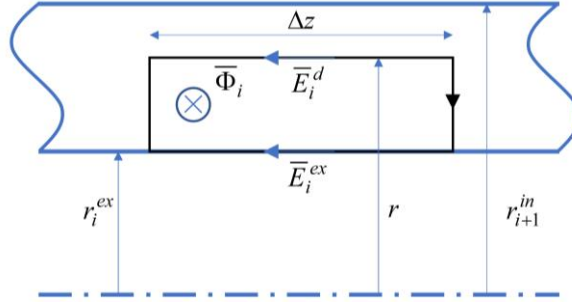


Fig. 2 Computation of electric field inside the dielectric layer between the i -th and $(i+1)$ -th conductive layers

The line integral reduces to the following expression since the values of electric field are constant along the integration curve and cancel each other out on parts of the curve perpendicular to the conductor axis:

$$\bar{E}_i^d - \bar{E}_i \Big|_{r=r_i^{ex}} = +j \cdot \omega \cdot \bar{\Phi}_i \quad (9)$$

The per-unit-length magnetic flux through the surface bounded by the integration curve depicted on Fig. 2 is easily obtained by integrating the magnetic flux density through the surface:

$$\bar{\Phi}_i = \mu_i^d \cdot \int_{r_i^{ex}}^r \bar{H}_i^d \cdot dr \cdot 1 = \mu_i^d \cdot r_i^{ex} \cdot \ell n \frac{r}{r_i^{ex}} \cdot \bar{H}_i \Big|_{r=r_i^{ex}} \quad (10)$$

where μ_i^d is the magnetic permeability of the dielectric layer located between the i -th and $(i+1)$ -th conductive layers.

By introducing (10) into (9) and rearranging the expression one can obtain the following expression for electric field inside the dielectric layer between the i -th and $(i+1)$ -th conductive layers:

$$\bar{E}_i^d = \bar{E}_i \Big|_{r=r_i^{ex}} + j \cdot \omega \cdot \mu_i^d \cdot r_i^{ex} \cdot \ell n \frac{r}{r_i^{ex}} \cdot \bar{H}_i \Big|_{r=r_i^{ex}} \quad (11)$$

Since the electric and magnetic fields inside dielectric layers are computed indirectly, the number of unknown complex-valued coefficients has been reduced unlike in paper [11] where each layer, be it conductive or dielectric, adds two unknowns to the subsequent system of equations. Computation of unknown coefficients slightly varies depending on whether the multilayer conductor is a solid conductor ($r_i^{in} = 0$) or a tubular conductor ($r_i^{in} \neq 0$). The computation of unknown complex-valued coefficients from the boundary conditions is given in Appendix A.

4. PER-UNIT-LENGTH INTERNAL IMPEDANCE OF THE MULTILAYER CONDUCTOR

Per-unit-length internal impedance of the multilayer conductor with possible dielectric layers where the displacement currents have been disregarded in the entire conductor is computed using the value of electric field on the outer edge of the multilayer conductor using the following expression:

$$\bar{Z} = \frac{\bar{E}_m|_{r=r_m^{ex}}}{\bar{I}_{tot}} = Z \cdot \exp(j \cdot \varphi) \quad (12)$$

where Z is the modulus of the per-unit-length internal impedance of the multilayer conductor and φ is the phase angle of the per-unit-length internal impedance of the multilayer conductor.

Substituting equation (4) into (12), one obtains the following expression for computation of per-unit-length impedance of the multilayer conductor:

$$\bar{Z} = \frac{\bar{\gamma}_m}{\sigma_m} \cdot \left\{ \bar{C}_m^s \cdot \bar{I}_0^s(\bar{\gamma}_m \cdot r_m) - \bar{D}_m^s \cdot \bar{K}_0^s(\bar{\gamma}_m \cdot r_m) \cdot \exp[-\bar{\gamma}_m \cdot (r_m^{ex} - r_m^{in})] \right\} \quad (13)$$

5. COMPARISON WITH A MODEL OF THE MULTILAYER CONDUCTOR FROM [11]

In paper [11], a model of a multilayer conductor is developed which consists of an arbitrary number of layers which can feature arbitrary electrical and magnetic parameters. This, in fact, means that each layer has its electrical conductivity, permittivity and magnetic permeability, hence conductive and displacement currents have been taken into account in all layers. In this paper, however, a different approach is proposed which totally disregards displacement currents in all layers. In following two examples, the effects of this will be investigated.

5.1. Example 1

In the first numerical example the following multilayer conductor with four layers in total is considered:

1. $r_1^{in} = 0$; $r_1^{ex} = 5$ mm; $\sigma_1 = 1.37$ MS/m; $\mu_1 = 1.02 \cdot \mu_0$; $\varepsilon_1 = \varepsilon_0$
2. $r_2^{in} = 5$ mm; $r_2^{ex} = 10$ mm; $\sigma_2 = 59.6$ MS/m; $\mu_2 = 0.999994 \cdot \mu_0$; $\varepsilon_2 = \varepsilon_0$
3. $r_3^{in} = 10$ mm; $r_3^{ex} = 15$ mm; $\sigma_3 = 0$; $\mu_3 = \mu_0$; $\varepsilon_3 = \varepsilon_0$
4. $r_4^{in} = 15$ mm; $r_4^{ex} = 20$ mm; $\sigma_4 = 10$ MS/m; $\mu_4 = \mu_0$; $\varepsilon_4 = \varepsilon_0$

As can be seen from the previous list, first two layers are conductive layers, the third layer is a dielectric layer, whereas the final layer is a conductive layer. These parameters have been implemented into the model from [11] which takes displacement currents into account in all layers, and into the proposed model where displacement currents have been disregarded.

Per-unit-length internal impedance is computed for a set of frequencies ranging from very low to very high frequencies. Fig. 3 depicts the moduli of the per-unit-length internal impedance for both models, whereas Fig. 4 depicts the phase angle of the impedance. As can be observed from both figures the curves coincide throughout the observation interval. The maximum difference between the moduli of per-unit-length internal impedances is

$1.0179 \cdot 10^{-10}$, whereas the maximum difference between the phase angles of per-unit-length internal impedances is $1.6209 \cdot 10^{-7}$.

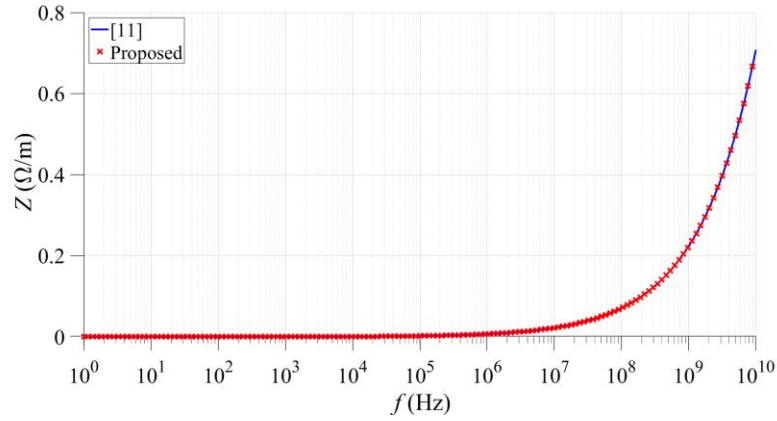


Fig. 3 Comparison of moduli of per-unit-length internal impedance computed by the model from [11] and the proposed model for the first example

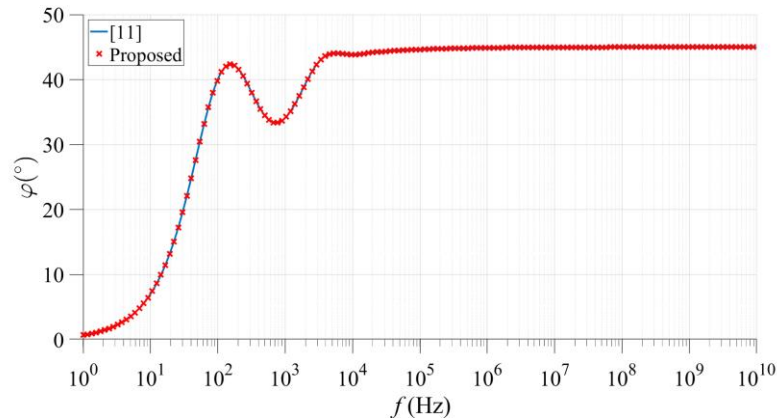


Fig. 4 Comparison of phase angles of per-unit-length internal impedance computed by the model from [11] and the proposed model for the first example

5.2. Example 2

In the second numerical example the following multilayer conductor with seven layers in total is considered. A tubular multilayer conductor consisting of four thin conductive layers and three dielectric layers is considered:

1. $r_1^{\text{in}} = 4$; $r_1^{\text{ex}} = 5$ mm; $\sigma_1 = 59.6$ MS/m; $\mu_1 = 0.999994 \cdot \mu_0$; $\varepsilon_1 = \varepsilon_0$
2. $r_2^{\text{in}} = 5$ mm; $r_2^{\text{ex}} = 7$ mm; $\sigma_2 = 0$; $\mu_2 = \mu_0$; $\varepsilon_2 = \varepsilon_0$
3. $r_3^{\text{in}} = 7$ mm; $r_3^{\text{ex}} = 8$ mm; $\sigma_3 = 1.37$ MS/m; $\mu_3 = 1.02 \cdot \mu_0$; $\varepsilon_3 = \varepsilon_0$
4. $r_4^{\text{in}} = 8$ mm; $r_4^{\text{ex}} = 10$ mm; $\sigma_4 = 0$; $\mu_4 = \mu_0$; $\varepsilon_4 = \varepsilon_0$
5. $r_5^{\text{in}} = 10$ mm; $r_5^{\text{ex}} = 11$ mm; $\sigma_5 = 10$ MS/m; $\mu_5 = \mu_0$; $\varepsilon_5 = \varepsilon_0$
6. $r_6^{\text{in}} = 11$ mm; $r_6^{\text{ex}} = 13$ mm; $\sigma_6 = 0$; $\mu_6 = \mu_0$; $\varepsilon_6 = \varepsilon_0$
7. $r_7^{\text{in}} = 13$ mm; $r_7^{\text{ex}} = 14$ mm; $\sigma_7 = 59.6$ MS/m; $\mu_7 = 0.999994 \cdot \mu_0$; $\varepsilon_7 = \varepsilon_0$

These parameters have been implemented into the model from [11] which takes displacement currents into account in all layers, and into the proposed model where displacement currents have been disregarded.

Per-unit-length internal impedance is computed for a set of frequencies ranging from very low to very high frequencies. Fig. 5 depicts the moduli of the per-unit-length internal impedance for both models, whereas Fig. 6 depicts the phase angle of the impedance. As can be observed from both figures the curves coincide throughout the observation interval. The maximum difference between the moduli of per-unit-length internal impedances is $1.1872 \cdot 10^{-10}$, whereas the maximum difference between the phase angles of per-unit-length internal impedances is $1.7847 \cdot 10^{-4}$.

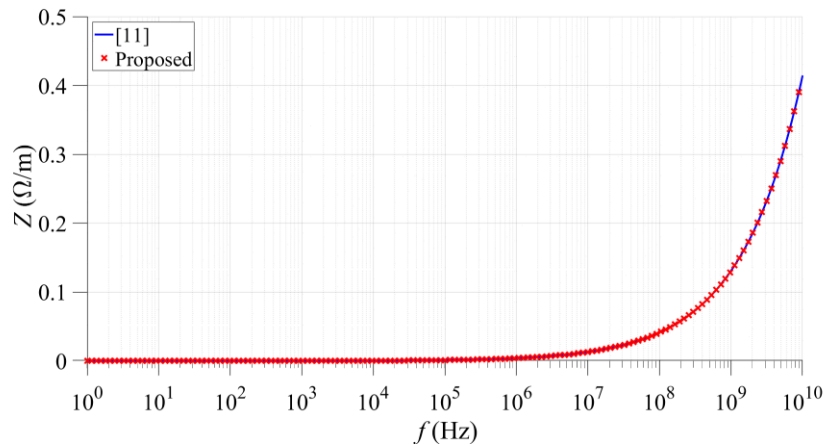


Fig. 5 Comparison of moduli of per-unit-length internal impedance computed by the model from [11] and the proposed model for the second example

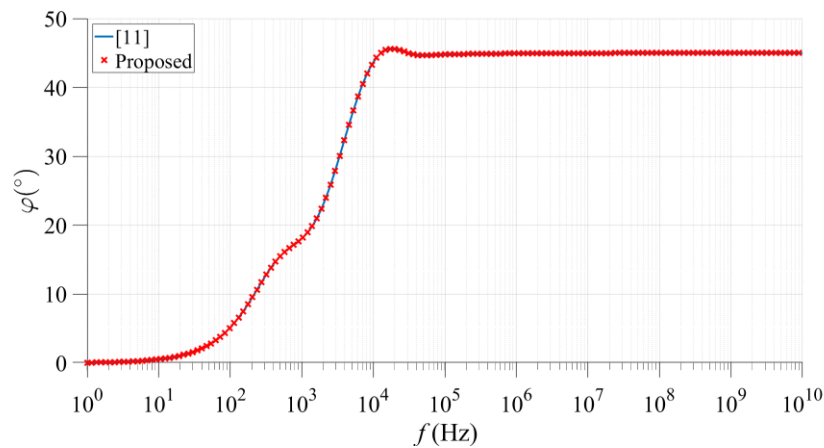


Fig. 6 Comparison of phase angles of per-unit-length internal impedance computed by the model from [11] and the proposed model for the second example

5.3. Discussion

Other than the presented two numerical examples, numerous comparisons have been made for different kinds of multilayer conductors and the authors came to the same conclusion. Disregarding the displacement currents in both the conductive layers and the dielectric layers introduces a practically insignificant error in the model if the conductive layers are good conductors. Furthermore, the number of unknowns in the system of equations is reduced since the dielectric layers are treated differently than in [11] which reduces computation time by approximately 23%. It can also be noted here that the model presented in [11] was tested against similar models available in the literature which are based on a cascade of a set of two-port networks [8-10] and proved equally accurate and far more stable. Therefore, by comparing the proposed model to the model presented in [11] one can also validate this proposed model relative to the other models available in literature.

6. CONCLUSION

In this paper a model of the multilayer conductor with conductive and dielectric layers is proposed. In the proposed model the effect of totally disregarding displacement currents in both conductive layers and dielectric layers was examined and the authors came to the conclusion that displacement currents have negligible effects on the distribution of electric and magnetic field inside a multilayered conductor even for higher frequency values. In addition to this, the dielectric layers are taken into account indirectly in a way that does not add additional unknown coefficients to the system of linear equations, which reduces computation time.

REFERENCES

- [1] S. Olsen, C. Traeholt, A. Kuhle, O. Tonnesen, M. Daumling, and J. Ostergaard, "Loss and inductance investigations in a 4-layer superconducting prototype cable conductor," *IEEE Transactions on Applied Superconductivity*, vol. 9, no. 2, pp. 833–836, 1999.
- [2] V. Morgan, "Effects of alternating and direct current, power frequency, temperature, and tension on the electrical parameters of ACSR conductors," *IEEE Transactions on Power Delivery*, vol. 18, no. 3, pp. 859–866, 2003.
- [3] Z. Zhihua, M. Weiming, "AC impedance of an isolated flat conductor," *IEEE Transactions on Electromagnetic Compatibility*, vol. 44, no. 3, pp. 482–486, 2002.
- [4] W. Mingli, F. Yu, "Numerical calculations of internal impedance of solid and tubular cylindrical conductors under large parameters," *IEE Proceedings - Generation, Transmission and Distribution*, vol. 151, no. 1, pp. 67–72, 2004.
- [5] G. A. Antonini, A. Orlandi, C. R. Paul, "Internal impedance of conductors of rectangular cross section," *IEEE Transactions on Microwave Theory and Techniques*, vol. 47, no. 7, pp. 979–985, 1999.
- [6] S. Vujević, P. Sarajčević, D. Lovrić, "Time-harmonic analysis of grounding system in horizontally stratified multilayer medium," *Electric Power Systems Research*, vol. 83, pp. 28–37, 2011.
- [7] L. Greev, F. Dawalibi, "An electromagnetic model for transients in grounding systems," *IEEE Transactions on Power Delivery*, vol. 5, pp. 1779–1781, 1990.
- [8] J. A. Brandao Faria, "A circuit approach for the electromagnetic analysis of inhomogeneous cylindrical structures," *Progress in Electromagnetics Research B*, vol. 30, pp. 223–238, 2011.
- [9] J. A. Brandao Faria, "A matrix approach for the evaluation of the internal impedance of multilayered cylindrical structures," *Progress in Electromagnetics Research B*, vol. 28, pp. 351–367, 2011.

- [10] K. Kubicek, M. Kampik, "Highly accurate and numerically stable matrix computations of the internal impedance of multilayer cylindrical conductors," *IEEE Transactions on Electromagnetic Compatibility*, vol. 62, no. 1, pp. 204–211, 2020.
- [11] S. Vujević, D. Lovrić, I. Krolo, I. Duvnjak, "Computation of electric and magnetic field distribution inside a multilayer cylindrical conductor," *Progress in Electromagnetics Research M*, vol. 88, pp. 53–63, 2020.
- [12] M. Abramowitz, I. A. Stegun, *Handbook of Mathematical Functions with Formulas, Graphs, and Mathematical Tables*, New York: Dover Publications, 1964.
- [13] S. Vujević, D. Lovrić, V. Boras, "High-accurate numerical computation of internal impedance of cylindrical conductors for complex arguments of arbitrary magnitude", *IEEE Transactions on Electromagnetic Compatibility*, vol. 56, pp. 1431–1438, 2014.
- [14] S. Vujević, D. Lovrić, "On the numerical computation of cylindrical conductor internal impedance for complex arguments of large magnitude", *Facta Universitatis Series: Electronics and Energetics*, vol. 30, no. 1, pp. 81–91, 2017.
- [15] D. Lovrić, S. Vujević, "Accurate computation of internal impedance of two-layer cylindrical conductors for arguments of arbitrary magnitude," *IEEE Transactions on Electromagnetic Compatibility*, vol. 60, no. 2, pp. 347–353, 2018.

APPENDIX A

FORMATION OF THE SYSTEM OF EQUATIONS FOR COMPUTING THE UNKNOWN COMPLEX-VALUED COEFFICIENTS

Model of the multilayer cylindrical conductor presented in this paper can have an arbitrary number of conductive layers (m). This means that there are $2 \cdot m$ unknown scaled complex-valued coefficients \bar{C}_i^s and \bar{D}_i^s ($i = 1, 2, \dots, m$) which one needs to compute in order to know the electric and magnetic field distribution in all layers. Unknown scaled complex-valued coefficients are obtained by forming and solving a system of $2 \cdot m$ linear equations which are derived from the boundary conditions between layers and the boundary conditions on the edges of the multilayer conductor.

The first $2 \cdot (m-1)$ equations in the system of equations are formed from the boundary conditions between layers requiring that the tangential components of electric field intensity and magnetic field intensity are continuous on border between two adjacent layers. The possible existence of a dielectric layer between two conductive layers is taken into account in the following boundary conditions, which are directly derived from equations (9) and (12) where in this case, r is substituted with r_{i+1}^{in} :

$$\bar{H}_i \Big|_{r=r_i^{ex}} = \frac{r_{i+1}^{in}}{r_i^{ex}} \cdot \bar{H}_{i+1} \Big|_{r=r_{i+1}^{in}} \quad ; \quad i = 1, 2, \dots, m-1 \quad (A1)$$

$$\bar{E}_i \Big|_{r=r_i^{ex}} + j \cdot \omega \cdot \mu_i^d \cdot r_i^{ex} \cdot \ell n \frac{r_{i+1}^{in}}{r_i^{ex}} \cdot \bar{H}_i \Big|_{r=r_i^{ex}} = \bar{E}_{i+1} \Big|_{r=r_{i+1}^{in}} \quad ; \quad i = 1, 2, \dots, m-1 \quad (A2)$$

Equations (A1-A2) are valid for both cases when the first conductive layer is a solid layer or if it is a tubular layer.

One additional equation, also valid for both cases, is derived from the boundary condition on the outer edge of the multilayer cylindrical conductor:

$$\bar{H}_m \Big|_{r=r_m^{ex}} = \frac{\bar{I}_{tot}}{2 \cdot \pi \cdot r_m^{ex}} \quad (A3)$$

The final equation in the system of equations varies for the cases of solid and tubular cylindrical conductors since it is derived from the innermost edge of the conductor (if it exists).

In the case where the first conductive layer is a **solid** cylindrical conductor, then obviously the internal radius of the first layer equals zero. Since modified Bessel functions of the second kind tend to infinity if their argument is zero, they must be eliminated in order to preserve the physical validity of results. In this case the final equation in the system of equations for the case of the solid cylindrical conductor is:

$$\bar{D}_1^s = 0 \quad (A4)$$

However, in the case where the first conductive layer is a **tubular** cylindrical conductor, then the internal radius of the first layer does not equal zero so no singularity issues occur. Hence, the boundary condition on the innermost edge of the conductor can be included as the final equation in the system of equations for the tubular cylindrical conductor:

$$\bar{H}_1 \Big|_{r=r_1^{in}} = 0 \quad (A5)$$

By introducing equations for electric and magnetic field described by (1-2) into (A1-A5), the following system of $2 \cdot m$ equations is obtained:

Equations 1 to 2·m-2:

$$\begin{aligned} & \bar{C}_i^s \cdot \bar{I}_1^s(\bar{\gamma}_i \cdot r_i^{ex}) + \bar{D}_i^s \cdot \bar{K}_1^s(\bar{\gamma}_i \cdot r_i^{ex}) \cdot \exp[-\bar{\gamma}_i \cdot (r_i^{ex} - r_i^{in})] \\ & - \bar{C}_{i+1}^s \cdot \bar{I}_1^s(\bar{\gamma}_{i+1} \cdot r_{i+1}^{in}) \cdot \frac{r_{i+1}^{in}}{r_i^{ex}} \cdot \exp[-\bar{\gamma}_{i+1} \cdot (r_{i+1}^{ex} - r_{i+1}^{in})] \\ & - \bar{D}_{i+1}^s \cdot \bar{K}_1^s(\bar{\gamma}_{i+1} \cdot r_{i+1}^{in}) \cdot \frac{r_{i+1}^{in}}{r_i^{ex}} = 0 ; i = 1, 2, \dots, m-1 \end{aligned} \quad (A6)$$

$$\begin{aligned} & \bar{C}_i^s \cdot \left[\bar{I}_0^s(\bar{\gamma}_i \cdot r_i^{ex}) + \bar{\gamma}_i \cdot r_i^{ex} \cdot \frac{\mu_i^d}{\mu_i} \cdot \ell n \frac{r_{i+1}^{in}}{r_i^{ex}} \cdot \bar{I}_1^s(\bar{\gamma}_i \cdot r_i^{ex}) \right] \\ & - \bar{D}_i^s \cdot \left[\bar{K}_0^s(\bar{\gamma}_i \cdot r_i^{ex}) - \bar{\gamma}_i \cdot r_i^{ex} \cdot \frac{\mu_i^d}{\mu_i} \cdot \ell n \frac{r_{i+1}^{in}}{r_i^{ex}} \cdot \bar{K}_1^s(\bar{\gamma}_i \cdot r_i^{ex}) \right] \cdot \exp[-\bar{\gamma}_i \cdot (r_i^{ex} - r_i^{in})] \\ & - \bar{C}_{i+1}^s \cdot \sqrt{\frac{\mu_{i+1} \cdot \sigma_i}{\mu_i \cdot \sigma_{i+1}}} \cdot \bar{I}_0^s(\bar{\gamma}_{i+1} \cdot r_{i+1}^{in}) \cdot \exp[-\bar{\gamma}_{i+1} \cdot (r_{i+1}^{ex} - r_{i+1}^{in})] \\ & + \bar{D}_{i+1}^s \cdot \sqrt{\frac{\mu_{i+1} \cdot \sigma_i}{\mu_i \cdot \sigma_{i+1}}} \cdot \bar{K}_0^s(\bar{\gamma}_{i+1} \cdot r_{i+1}^{in}) = 0 ; i = 1, 2, \dots, m-1 \end{aligned} \quad (A7)$$

Equation 2·m-1:

$$\bar{C}_m^s \cdot \bar{I}_1^s(\bar{\gamma}_m \cdot r_m^{ex}) + \bar{D}_m^s \cdot \bar{K}_1^s(\bar{\gamma}_m \cdot r_m^{ex}) \cdot \exp[-\bar{\gamma}_m \cdot (r_m^{ex} - r_m^{in})] = \frac{1}{2 \cdot \pi \cdot r_m^{ex}} \quad (\text{A8})$$

Equation 2·m:

$$\bar{C}_1^s \cdot \bar{I}_1^s(\bar{\gamma}_1 \cdot r_1^{in}) \cdot \exp[-\bar{\gamma}_1 \cdot (r_1^{ex} - r_1^{in})] + \bar{D}_1^s \cdot \bar{K}_1^s(\bar{\gamma}_1 \cdot r_1^{in}) = 0 \quad (\text{A9})$$

or

$$\bar{D}_1^s = 0 \quad (\text{A10})$$